

Linearly implicit methods for a semilinear parabolic system arising in two-phase flows

GEORGIOS AKRIVIS[†]

*Computer Science Department, University of Ioannina,
451 10 Ioannina, Greece.*

DEMETRIOS T. PAPAGEORGIOU[‡]

*Department of Mathematics, Imperial College London,
London, SW7 2AZ, UK.*

YIORGOS-SOKRATIS SMYRLIS[§]

*Department of Mathematics and Statistics, University of Cyprus,
P. O. Box 20537, 1678 Nicosia, Cyprus.*

[Received on January 15, 2009]

We study the discretization of a nonlinear parabolic system arising in two-phase flows, which in a special case reduces to the Kuramoto–Sivashinsky equation, by linearly implicit methods, and in particular by implicit–explicit multistep methods. We carry out extensive numerical experiments to investigate the accuracy and efficiency of these algorithms with extremely satisfactory results. These numerical experiments establish the analyticity of the solution and the existence of global attractors (rigorous proofs of such results for this system are not available). Our numerical experiments yield a sharp estimate for the band of analyticity of the solutions as the parameters vary. The accuracy of the schemes enables, in general, the exhaustive numerical study of such systems and the full classification of the inertial manifold. We provide numerical examples of travelling time-periodic attractors as well as quasi-periodic and chaotic attractors.

Keywords: Semilinear parabolic systems, linearly implicit schemes, implicit–explicit BDF schemes, dissipative infinite dimensional dynamical systems, Kuramoto–Sivashinsky equation.

1. Introduction

We consider the following parabolic system

$$(1.1) \quad \begin{cases} H_t + H_{xxx} + H_{xx} + HH_x + \Gamma_{xx} = 0, \\ \Gamma_t - \eta \Gamma_{xx} + (H\Gamma)_x = 0, \end{cases}$$

where $(x, t) \in \mathbb{R} \times [0, \infty)$. Here, the functions $H = H(x, t)$ and $\Gamma = \Gamma(x, t)$ are L -periodic in the space variable x , and η is a positive diffusion constant. Our objectives are twofold: first, to discretize initial value problems for the nonlinear parabolic system (1.1) in time by the wide class of linearly implicit methods of Akrivis & Crouzeix (2004) (see also Akrivis *et al* 1999); second, to use these algorithms to

[†]Email: akrivis@cs.uoi.gr

[‡]Email: d.papageorgiou@imperial.ac.uk

[§]Email: smyrlis@ucy.ac.cy

accurately compute solutions of the system (1.1) and to provide numerical evidence for the analyticity of solutions. We establish numerically that (1.1) is a dissipative infinite-dimensional dynamical system and provide a classification and description of different large-time attractors.

The system (1.1) arises in the spatiotemporal evolution of core–annular flows when surfactants are present. Core–annular flows are two–phase flows in cylindrical tubes; the fluids typically arrange themselves so that one coats the cylindrical walls (the annular fluid) while the second immiscible fluid occupies the central core region. These flows are technologically important because they can act to “lubricate” the motion of a highly viscous core fluid (e.g., oil) with an annular layer of less viscous fluid (e.g., water). Applications abound in the oil and food industries, for example – see Joseph & Renardy (1993). The sharp interface between the two phases evolves nonlinearly and provides a moving boundary problem. The system (1.1) was derived asymptotically by Kas–Danouche *et al* (2009), starting from the Navier–Stokes equations and assuming a small annular layer thickness. The dependent variable H corresponds to the scaled interfacial shape and Γ is the local surfactant concentration at the interface. Surfactants change the surface tension coefficient and the system (1.1) allows for such effects through the coupling between the two equations. Kas–Danouche *et al* provide numerical solutions that predict nonlinear travelling waves as well as complicated dynamics including quasi–periodic and chaotic flows.

In the absence of surfactants, the surface tension is constant and the system (1.1) reduces to the Kuramoto–Sivashinsky (KS) equation (we write $u(x, t) = H(x, t)$ in this case),

$$(1.2) \quad u_t + uu_x + u_{xx} + u_{xxx} = 0 \text{ in } \mathbb{R} \times [0, \infty),$$

which has received considerable attention both analytically and computationally. (More specifically, the constant surface tension case derives from the limit $\eta \rightarrow \infty$ – see Kas–Danouche *et al* 2009.) The KS equation is one of the simplest PDEs that can produce complex chaotic dynamics (see, for example, Hyman & Nicolaenko (1988); Hyman *et al* (1986); Jolly *et al* (1990); Kevrekidis *et al* (1990); Papageorgiou & Smyrlis (1991); Smyrlis & Papageorgiou 1991, 1996) and it has been shown numerically that routes to chaos follow the Feigenbaum universal theory of a period–doubling cascade (see Smyrlis & Papageorgiou 1991 where the Feigenbaum universal constants are also calculated to three decimals). All these computations provided considerable evidence for the low–modal behavior of the KS and indeed the existence of finite dimensional inertial manifolds. A considerable corpus of analytical results exist for the KS and we review some of the most salient ones needed for our purposes here. It is shown by Constantin *et al* (1989) that the long–time dynamics of KS is governed by a finite dimensional dynamical system of size at least as large as the number of linearly unstable modes which are equal to $[L/2\pi]$ for L –periodic solutions. For general initial data we have boundedness of solutions as shown independently by Il’yashenko (1992), Goodman (1994) and Collet *et al* (1993b). In particular it is estimated by Collet *et al* (1993b) that the Hausdorff dimension of the attractor satisfies

$$(1.3) \quad \limsup_{t \rightarrow \infty} \|u(\cdot, t)\| \leq CL^{8/5},$$

where C is a generic constant and $\|\cdot\|$ is the L^2 –norm of L –periodic functions. The result (1.3) can be used in turn to prove boundedness of the solution in any Sobolev norm – see references. In a companion paper Collet *et al* (1993a) prove results on the analyticity of solutions to KS. They show that at large times the solution is analytic in a strip of size $\beta \geq cL^{-16/25}$ around the real axis, where c is a constant independent of L . This provides the following estimate for the spectral density at high wavenumbers,

$$(1.4) \quad \limsup_{t \rightarrow \infty} |\hat{u}(j, t)| = \mathcal{O}(e^{-cL^{-16/25}q|j|}),$$

where $\hat{u}(j, t)$ is the j th Fourier coefficient of $u(\cdot, t)$ and $q = 2\pi/L$. Results such as (1.4) are not sharp as revealed by the numerical experiments of Collet *et al* (1993a). It is found that a much better bound exists of the form

$$(1.5) \quad \limsup_{t \rightarrow \infty} \sum_{j \in \mathbb{Z}} e^{2\beta q|j|} |\hat{u}(j, t)|^2 < \infty,$$

where $\beta > 0$ is independent of L , and numerical experiments indicate that $\beta \approx 3.5$.

The KS equation has been shown to be amenable to computer assisted proofs. In particular, Zgliczyński and Mischaikow (2001) established the existence of stable stationary solutions of the KS equation for odd-parity initial data while Zgliczyński established the existence of periodic attractors of the KS equation in Zgliczyński (2004); in both works, the numerical evidence of existence of such attractors in the corresponding truncated system was used as an assumption. Dieci *et al* (2008) analyze the error in approximating Lyapunov exponents of dissipative dynamical systems on inertial manifolds using QR techniques and give results for the KS equation as an example. They also calculate evidence of chaotic attractors by use of the Kaplan–Yorke dimension.

The theoretical results reviewed above for the KS equation do not have their analogues for the system (1.1) (in fact, we are unaware of rigorous analytical work on systems of KS–type equations). Uniqueness of smooth solutions is easily proved but we do not have results regarding boundedness and estimates of the Hausdorff dimension of attractors, or rigorous estimates for the size of the strip of analyticity when the solutions are analytic. We will explore such questions numerically using the schemes developed here.

In the sequel we rescale system (1.1) from L - to 2π -periodic domains by the transformations $x = (L/2\pi)x_1$, $t = (1/\nu)t_1$, $H = \nu^{1/2}H_1$ and $\Gamma = \nu^{1/2}\Gamma_1$, where $\nu = 4\pi^2/L^2$. The resulting system becomes (dropping the subscripts 1)

$$(1.6) \quad \begin{cases} H_t + \nu H_{xxxx} + H_{xx} + HH_x + \Gamma_{xx} = 0, \\ \Gamma_t - \eta \Gamma_{xx} + (H\Gamma)_x = 0, \end{cases}$$

where $(x, t) \in \mathbb{R} \times [0, \infty)$. The remainder of the article is concerned with the canonical system (1.6).

There are two parameters present, ν and η , and the limit $\nu \rightarrow 0$ is excluded because the equations become semilinear PDEs with negative diffusion and hence are ill-posed (this limit is also excluded on physical grounds). The limit $\eta = 0$, however, produces a coupled system of a KS–type equation with a conservation law and the behavior of such systems are quite distinct from the dissipative inertial manifold behavior of KS.

An outline of the paper is as follows. Section 2 is devoted to the discretization of (1.6) by implicit–explicit BDF schemes in time and by spectral methods in space; we establish optimal order error estimates. In Section 3 we present numerical experiments which establish the p th order accuracy of the p -step scheme; to this end we apply the schemes to a suitably modified *inhomogeneous* system with known exact solution. Specific experiments are carried out in order to assess the number of modes to be used as the value of ν varies, to demonstrate that the solution is analytic and to compute the band of analyticity. Extensive numerical tests have been carried out to evaluate certain quantitative characteristics of the global attractors of the system. Finally, in Section 4 we present our conclusions.

2. Numerical analysis for implicit–explicit BDF schemes for the semilinear parabolic system

This section is devoted to the discretization of (1.6) by linearly implicit methods. We first rewrite (1.6) in an appropriate form to cast it in the class of equations discretized in Akrivis & Crouzeix (2004) by

linearly implicit methods in time; see also Akrivis *et al* (1999). We then show that the conditions posed in Akrivis & Crouzeix (2004) are indeed fulfilled. Subsequently, we discretize (1.6) by a subclass of the methods considered in Akrivis & Crouzeix (2004), namely by implicit–explicit BDF schemes. Finally, we combine the discretization in time with spectral methods for the space discretization to construct fully discrete, implementable numerical schemes.

2.1 Preliminaries

Our goal here is to rewrite (1.6) in an appropriate form to fit in the class of abstract equations discretized in Akrivis & Crouzeix (2004) and show that all conditions of Akrivis & Crouzeix (2004) are indeed satisfied. This will then allow discretization in time by linearly implicit schemes.

For reasons that will become apparent in the sequel, we write (1.6) as

$$(2.1) \quad \begin{cases} H_t + \nu H_{xxxx} + H_{xx} + \frac{1}{\nu} H = -HH_x + \frac{1}{\nu} H - \Gamma_{xx}, \\ \Gamma_t - \eta(\Gamma_{xx} - \Gamma) = -(H\Gamma)_x + \eta\Gamma, \end{cases}$$

where $(x, t) \in \mathbb{R} \times [0, \infty)$. We write (2.1) in the form

$$(2.2) \quad \mathbf{u}_t + \mathbf{A}\mathbf{u} = \mathbf{B}(\mathbf{u}) \quad \text{in } \mathbb{R} \times [0, \infty).$$

in an appropriate Hilbert space setting and will check that the linear operator \mathbf{A} is self-adjoint and positive definite and the nonlinear operator \mathbf{B} is locally Lipschitz continuous; thus the conditions in Akrivis & Crouzeix (2004) are fulfilled and the system can be discretized by linearly implicit methods (Akrivis *et al* 1998, Akrivis *et al* 1999 and Akrivis & Crouzeix 2004).

For $s \in \mathbb{N}_0$, let H_{per}^s denote the periodic Sobolev space of order s , consisting of the 2π -periodic elements of $H_{\text{loc}}^s(\mathbb{R})$, and let $\|\cdot\|_{H^s}$ be the norm over a period in H_{per}^s . The inner product in $L_{\text{per}}^2 = H_{\text{per}}^0$ is denoted by (\cdot, \cdot) and the induced norm by $\|\cdot\|$. We introduce the linear operators $A_1 : H_{\text{per}}^4 \rightarrow L_{\text{per}}^2$ and $A_2 : H_{\text{per}}^2 \rightarrow L_{\text{per}}^2$ by

$$A_1 v := \nu v_{xxxx} + v_{xx} + \frac{1}{\nu} v, \quad A_2 v := -\eta(v_{xx} - v).$$

Obviously, both A_1 and A_2 are selfadjoint. Furthermore, it is easily seen that

$$(2.3) \quad (A_1 v, v) \geq \frac{1}{2} (v \|v_{xx}\|^2 + \frac{1}{\nu} \|v\|^2) \quad \text{for all } v \in H_{\text{per}}^2$$

and

$$(2.4) \quad (A_2 v, v) = \eta (\|v_x\|^2 + \|v\|^2) \quad \forall v \in H_{\text{per}}^1.$$

Hence, A_1 and A_2 are positive definite. Here and in the sequel we also denote by (\cdot, \cdot) the duality pairing between H_{per}^{-1} and H_{per}^1 , as well as between H_{per}^{-2} and H_{per}^2 .

Let $\mathbf{H} := L_{\text{per}}^2 \times L_{\text{per}}^2$ and denote by $\langle \cdot, \cdot \rangle$ the product inner product,

$$\langle \mathbf{u}, \mathbf{v} \rangle := (u_1, v_1) + (u_2, v_2),$$

with $u_1, u_2, v_1, v_2 \in L_{\text{per}}^2$ the components of \mathbf{u} and \mathbf{v} , respectively. To formulate our problem in the form (2.2) in the framework of the Hilbert space $(\mathbf{H}, \langle \cdot, \cdot \rangle)$, we introduce the operator $\mathbf{A} : \mathcal{D}(\mathbf{A}) = H_{\text{per}}^4 \times H_{\text{per}}^2 \rightarrow \mathbf{H}$,

$$\mathbf{A}\mathbf{u} := \begin{pmatrix} A_1 & 0 \\ 0 & A_2 \end{pmatrix} \begin{pmatrix} u_1 \\ u_2 \end{pmatrix} = \begin{pmatrix} A_1 u_1 \\ A_2 u_2 \end{pmatrix}.$$

Obviously, \mathbf{A} is selfadjoint and positive definite. Let $\mathbf{W} := \mathcal{D}(\mathbf{A}^{1/2}) = H_{\text{per}}^2 \times H_{\text{per}}^1$ and \mathbf{V}' be the dual of \mathbf{V} , $\mathbf{V}' = H_{\text{per}}^{-2} \times H_{\text{per}}^{-1}$. We denote the norms in \mathbf{V} and \mathbf{V}' by $\|\cdot\|$ and $\|\cdot\|_*$, respectively,

$$\|\mathbf{u}\| = (\|A_1^{1/2}u_1\|^2 + \|A_2^{1/2}u_2\|^2)^{1/2}, \quad \|\mathbf{u}\|_* = (\|A_1^{-1/2}u_1\|^2 + \|A_2^{-1/2}u_2\|^2)^{1/2}.$$

Furthermore, let $\mathbf{B} : \mathcal{D}(A) \rightarrow \mathbf{H}$,

$$\mathbf{B}(\mathbf{u}) := - \begin{pmatrix} u_1(u_1)_x - \frac{1}{v}u_1 + (u_2)_{xx} \\ (u_1u_2)_x - \eta u_2 \end{pmatrix}.$$

Obviously, \mathbf{B} can be extended to a map from \mathbf{V} to \mathbf{V}' . With this notation, and $u_1 = H, u_2 = \Gamma$, the system (2.1) can be written in the form (2.2).

Our next task is to check the Lipschitz condition for the nonlinearity \mathbf{B} . For $\mathbf{v}, \tilde{\mathbf{v}}, \mathbf{w} \in \mathbf{V}$, we have,

$$\begin{aligned} \langle \mathbf{B}(\mathbf{v}) - \mathbf{B}(\tilde{\mathbf{v}}), \mathbf{w} \rangle &= -\frac{1}{2}((v_1^2 - \tilde{v}_1^2)_x, w_1) + \frac{1}{v}(v_1 - \tilde{v}_1, w_1) - ((v_2 - \tilde{v}_2)_{xx}, w_1) \\ &\quad - ((v_1v_2 - \tilde{v}_1\tilde{v}_2)_x, w_2) + \eta(v_2 - \tilde{v}_2, w_2) \\ &= \frac{1}{2}((v_1^2 - \tilde{v}_1^2), (w_1)_x) + \frac{1}{v}(v_1 - \tilde{v}_1, w_1) - (v_2 - \tilde{v}_2, (w_1)_{xx}) \\ &\quad + (v_1v_2 - \tilde{v}_1\tilde{v}_2, (w_2)_x) + \eta(v_2 - \tilde{v}_2, w_2). \end{aligned}$$

Therefore,

$$\begin{aligned} |\langle \mathbf{B}(\mathbf{v}) - \mathbf{B}(\tilde{\mathbf{v}}), \mathbf{w} \rangle| &\leq \frac{1}{2}\|v_1 + \tilde{v}_1\| \|(w_1)_x\|_{L^\infty} \|v_1 - \tilde{v}_1\| + \frac{1}{v}\|v_1 - \tilde{v}_1\| \|w_1\| \\ (2.5) \quad &\quad + \|v_2 - \tilde{v}_2\| \|(w_1)_{xx}\| + \eta\|v_2 - \tilde{v}_2\| \|w_2\| \\ &\quad + (\|v_2\|_{L^\infty} \|v_1 - \tilde{v}_1\| + \|\tilde{v}_1\|_{L^\infty} \|v_2 - \tilde{v}_2\|) \|(w_2)_x\|. \end{aligned}$$

Now, since $(w_1)_x$ vanishes at some point in the interval $(0, 2\pi)$, it is easily seen that

$$\|(w_1)_x\|_{L^\infty} \leq \sqrt{2\pi} \|(w_1)_{xx}\|$$

and (2.5) yields

$$\begin{aligned} |\langle \mathbf{B}(\mathbf{v}) - \mathbf{B}(\tilde{\mathbf{v}}), \mathbf{w} \rangle| &\leq \left(\frac{\sqrt{2\pi}}{2} + \|v_1 + \tilde{v}_1\| \right) \|v_1 - \tilde{v}_1\| \|(w_1)_{xx}\| \\ (2.6) \quad &\quad + \frac{1}{v}\|v_1 - \tilde{v}_1\| \|w_1\| + \eta\|v_2 - \tilde{v}_2\| \|w_2\| \\ &\quad + (\|v_2\|_{L^\infty} \|v_1 - \tilde{v}_1\| + \|\tilde{v}_1\|_{L^\infty} \|v_2 - \tilde{v}_2\|) \|(w_2)_x\|. \end{aligned}$$

Assume now that the components of the exact solution for a periodic initial value problem for (2.2) are bounded in $L^\infty(\mathbb{R})$, uniformly in time. Let \mathbf{T}_u be a tube around the solution \mathbf{u} , defined in terms of the L^∞ -norm,

$$\mathbf{T}_u := \{ \mathbf{v} \in \mathbf{V} : \inf_{t \geq 0} \|u_i(t) - v_i\|_{L^\infty} \leq 1, i = 1, 2 \}.$$

Taking into account the fact that

$$\|\mathbf{w}\| \geq \left(\frac{1}{2}(v\|(w_1)_{xx}\|^2 + \frac{1}{v}\|w_1\|^2) + \eta(\|(w_2)_x\|^2 + \|w_2\|^2) \right)^{1/2},$$

we easily conclude from (2.6)

$$(2.7) \quad \|\mathbf{B}(\mathbf{v}) - \mathbf{B}(\tilde{\mathbf{v}})\|_* \leq C \|\mathbf{v} - \tilde{\mathbf{v}}\| \quad \text{for all } \mathbf{v}, \tilde{\mathbf{v}} \in \mathbf{T}_{\mathbf{u}};$$

here $\|\cdot\|$ is the norm induced by the product L^2 inner product and the constant C depends on ν, η and the upper bound of the L^∞ -norm of the components of the exact solution \mathbf{u} .

REMARK 2.1 Using the properties of \mathbf{A} and the Lipschitz condition (2.7), we can easily establish uniqueness of smooth solutions for initial value problems for the system (2.2).

2.2 Implicit–explicit BDF schemes

In subsection 2.1 we checked all assumptions of Akrivis & Crouzeix (2004), see also Akrivis *et al* (1999); therefore, the linearly implicit schemes analyzed in Akrivis & Crouzeix (2004) can be used for the discretization in time of periodic initial value problems for (2.2). For concreteness, we focus here on some special implicit–explicit multistep methods, namely the implicit–explicit BDF schemes.

For $p \in \{1, \dots, 6\}$, let the polynomials α, β and γ be given by

$$(2.8) \quad \alpha(\zeta) := \sum_{j=1}^p \frac{1}{j} \zeta^{p-j} (\zeta - 1)^j, \quad \beta(\zeta) := \zeta^p \quad \text{and} \quad \gamma(\zeta) := \zeta^p - (\zeta - 1)^p.$$

The (α, β) -scheme described by the polynomials α and β is the p -step BDF scheme; these schemes are strongly $A(0)$ -stable and will be used for the discretization of the linear part of (2.2). The explicit scheme (α, γ) will be used for the discretization of the nonlinear part of (2.2). Let us note that the order of both schemes, (α, β) and (α, γ) , is p .

Let $T > 0$ and consider the initial value problem

$$(2.9) \quad \begin{cases} \mathbf{u}_t + \mathbf{A}\mathbf{u} = \mathbf{B}(\mathbf{u}) & \text{in } \mathbb{R} \times (0, T), \\ \mathbf{u}(0) = \mathbf{u}^0, \end{cases}$$

with initial value $\mathbf{u}^0 \in \mathbf{H}$. Let $N \in \mathbb{N}$, $k := T/N$ be the constant time step and $t^n, t^n := nk, n = 0, \dots, N$, be the time levels at which we will approximate the solution \mathbf{u} . We use the (α, β, γ) -scheme to define approximations \mathbf{U}^n to $\mathbf{u}(\cdot, t^n)$ by

$$(2.10) \quad \sum_{i=0}^p \alpha_i \mathbf{U}^{n+i} + k\mathbf{A}\mathbf{U}^{n+p} = k \sum_{i=0}^{p-1} \gamma_i \mathbf{B}(\mathbf{U}^{n+i}), \quad n = 0, \dots, N-p,$$

for given starting approximations $\mathbf{U}^0, \dots, \mathbf{U}^{p-1}$, where α_i and γ_i denote the coefficients of ζ^i of the polynomials α and γ , respectively. Since $\alpha_p > 0$ and the operator \mathbf{A} is positive definite, the approximations $\mathbf{U}^p, \dots, \mathbf{U}^N$ are well defined by (2.10). For $p = 1$ the scheme (2.10) is single-step and reduces to the implicit–explicit Euler method,

$$(2.11) \quad \mathbf{U}^{n+1} + k\mathbf{A}\mathbf{U}^{n+1} = \mathbf{U}^n + k\mathbf{B}(\mathbf{U}^n), \quad n = 0, \dots, N-1.$$

Here, only one starting approximation, namely \mathbf{U}^0 , is needed, and we can take it equal to the exact initial value \mathbf{u}^0 . Let us also give the two-step scheme (2.10):

$$(2.12) \quad \frac{3}{2}\mathbf{U}^{n+2} + k\mathbf{A}\mathbf{U}^{n+2} = 2\mathbf{U}^{n+1} - \frac{1}{2}\mathbf{U}^n + 2k\mathbf{B}(\mathbf{U}^{n+1}) - k\mathbf{B}(\mathbf{U}^n), \quad n = 0, \dots, N-2.$$

Again, we can choose $\mathbf{U}^0 := \mathbf{u}^0$ and can compute an appropriate approximation \mathbf{U}^1 by performing one step of the implicit–explicit Euler method, $\mathbf{U}^1 + k\mathbf{A}\mathbf{U}^1 = \mathbf{U}^0 + k\mathbf{B}(\mathbf{U}^0)$.

For completeness we provide the list of all six BDF schemes in the Appendix.

According to Theorem 4.1 and Remark 7.2 of Akrivis & Crouzeix (2004), we have the following error estimate:

THEOREM 2.1 Let the solution \mathbf{u} of (2.9) be sufficiently smooth. Assume we are given starting approximations $\mathbf{U}^0, \mathbf{U}^1, \dots, \mathbf{U}^{p-1} \in \mathbf{V} \cap \mathbf{T}_u$ to $\mathbf{u}^0, \dots, \mathbf{u}^{p-1}$ such that

$$(2.13) \quad \max_{0 \leq j \leq p-1} \|\mathbf{u}(\cdot, t^j) - \mathbf{U}^j\| \leq Ck^p.$$

Let $\mathbf{U}^n \in \mathbf{V}, n = p, \dots, N$, be recursively defined by (2.10). Then, there exists a constant C , independent of k , such that, for k sufficiently small,

$$\max_{0 \leq n \leq N} \|\mathbf{u}(\cdot, t^n) - \mathbf{U}^n\| \leq Ck^p. \quad \square$$

2.3 Fully discrete schemes

To obtain computable approximations, we combine here the discretization in time by BDF schemes analyzed in the previous subsection with discretization in space. The space discretization is based on spectral methods. We establish optimal order error estimates.

Let $M \in \mathbb{N}$ and $S_M = \text{span}\{\varphi_{-M+1}, \dots, \varphi_M\}$, with $\varphi_\ell(x) := e^{i\ell x}$. Let $P_M : H_{\text{per}}^{-2} \rightarrow S_M$ denote the orthogonal L^2 –projection operator onto S_M , i.e.,

$$(v - P_M v, \chi) = 0 \quad \forall \chi \in S_M.$$

If we expand v in a Fourier series,

$$v = \sum_{\ell=-\infty}^{\infty} \hat{v}_\ell \varphi_\ell,$$

then $P_M v$ corresponds to the partial sum

$$P_M v = \sum_{\ell=-M+1}^M \hat{v}_\ell \varphi_\ell.$$

This projection has the following approximation property: *There exists a constant c , independent of v and M , such that, for $v \in H_{\text{per}}^m$ and $\ell = 0, \dots, m$,*

$$(2.14) \quad \|v - P_M v\|_{H_{\text{per}}^\ell} \leq cM^{\ell-m} \|v^{(m)}\|_{L_{\text{per}}^2}.$$

Since differentiation commutes with P_M , we have $P_M A_i = A_i P_M, i = 1, 2$. Furthermore, we let

$$\mathbf{P}_M := \begin{pmatrix} P_M & 0 \\ 0 & P_M \end{pmatrix}$$

and $\mathbf{S}_M := S_M \times S_M$, and define the finite rank operator $\mathbf{B}_M : \mathcal{D}(\mathbf{A}) \rightarrow \mathbf{S}_M, \mathbf{B}_M := \mathbf{P}_M \mathbf{B}$.

In the *semidiscrete* problem corresponding to (2.9) we seek a function $\mathbf{u}_M, \mathbf{u}_M(\cdot, t)$ in \mathbf{S}_M , satisfying

$$(2.15) \quad \begin{cases} \partial_t \mathbf{u}_M(\cdot, t) + \mathbf{A} \mathbf{u}_M(\cdot, t) = \mathbf{B}_M(\mathbf{u}_M(\cdot, t)), & 0 < t < T, \\ \mathbf{u}_M(\cdot, 0) = \mathbf{u}_M^0, \end{cases}$$

with $\mathbf{u}_M^0 \in \mathcal{S}_M$ a given approximation to \mathbf{u}^0 . We discretize (2.15) in time by implicit–explicit BDF schemes to construct fully discrete methods.

We recursively define a sequence of approximations $\mathbf{W}^\ell \in \mathcal{S}_M$ to $\mathbf{u}(\cdot, t^\ell)$ by

$$(2.16) \quad \sum_{i=0}^p \alpha_i \mathbf{U}^{n+i} + k \mathbf{A} \mathbf{U}^{n+p} = k \sum_{i=0}^{p-1} \gamma_i \mathbf{B}_M(\mathbf{U}^{n+i}).$$

Let $\mathbf{W}(\cdot, t) \in \mathcal{S}_M$ denote the L^2 –projection of $\mathbf{u}(\cdot, t)$ in \mathcal{S}_M , $\mathbf{W}(\cdot, t) = \mathbf{P}_M \mathbf{u}(\cdot, t)$, $t \in [0, T]$.

Let $\mathbf{E}_M(t) \in \mathcal{S}_M$ denote the consistency error of the semidiscrete equation (2.15) for \mathbf{W} ,

$$(2.17) \quad \mathbf{E}_M(t) := \mathbf{W}_t(\cdot, t) + \mathbf{A} \mathbf{W}(\cdot, t) - \mathbf{B}_M(\mathbf{W}(\cdot, t)), \quad t \in [0, T].$$

Obviously,

$$\mathbf{E}_M(t) = \mathbf{W}_t(\cdot, t) + \mathbf{P}_M \mathbf{A} \mathbf{u}(\cdot, t) - \mathbf{P}_M \mathbf{B}(\mathbf{W}(\cdot, t)),$$

whence, in view of the differential equation (2.9),

$$\mathbf{E}_M(t) = \mathbf{P}_M [\mathbf{B}(\mathbf{u}(\cdot, t)) - \mathbf{B}(\mathbf{W}(\cdot, t))].$$

Now, as a consequence of (2.14), $\mathbf{W}(\cdot, t) \in \mathbf{T}_u$, $t \in [0, T]$, and thus, in view of (2.7) and (2.14), under obvious regularity assumptions, we easily obtain the following optimal order estimate for the consistency error \mathbf{E}_M ,

$$(2.18) \quad \max_{0 \leq t \leq T} \|\mathbf{E}_M(t)\|_* \leq C(\mathbf{u}) M^{-m}.$$

Let us also note that, for $v \in H_{\text{per}}^1$,

$$|[v(x)]^2 - [v(y)]^2| = \left| 2 \int_x^y v(s) v'(s) ds \right| \leq 2 \|v\| \|v'\|,$$

whence

$$(2.19) \quad \|v\|_{L^\infty}^2 \leq \frac{1}{2\pi} \|v\|^2 + 2 \|v\| \|v'\|.$$

We can now derive an optimal order error estimate:

THEOREM 2.2 Assume that $\mathbf{U}^0, \mathbf{U}^1, \dots, \mathbf{U}^{p-1} \in \mathcal{S}_M$ are starting approximations to $\mathbf{u}(\cdot, t^0), \dots, \mathbf{u}(\cdot, t^{p-1})$ such that

$$(2.20) \quad \max_{0 \leq j \leq p-1} \|\mathbf{u}(\cdot, t^j) - \mathbf{U}^j\| \leq c(k^p + M^{-m})$$

and

$$(2.21) \quad \max_{0 \leq j \leq p-1} \|\mathbf{u}_i(\cdot, t^j) - \mathbf{U}_i^j\|_{L^\infty} \leq 1, \quad i = 1, 2.$$

Let $\mathbf{U}^n \in \mathcal{S}_M$, $n = p, \dots, N$, be recursively defined by (2.16). Then, if the solution \mathbf{u} of (2.9) is sufficiently smooth, there exists a constant C , independent of k and M , such that, for k sufficiently small and $M^{4m} k$ sufficiently large,

$$(2.22) \quad \max_{0 \leq n \leq N} \|\mathbf{u}(\cdot, t^n) - \mathbf{U}^n\| \leq C(k^p + M^{-m}).$$

Proof. First of all, in view of (2.14), we have

$$(2.23) \quad \max_{0 \leq n \leq N} \|\mathbf{u}(\cdot, t^n) - \mathbf{W}(\cdot, t^n)\| \leq cM^{-m}$$

and, also, for M sufficiently large,

$$(2.24) \quad \max_{0 \leq n \leq N} \|\mathbf{u}_i(\cdot, t^n) - \mathbf{W}_i(\cdot, t^n)\| \leq \frac{1}{4}, \quad i = 1, 2.$$

We next let $\tilde{\mathbf{W}}^j := \mathbf{W}(\cdot, t^j)$, $j = 0, \dots, p-1$, and define $\tilde{\mathbf{W}}^n \in \mathcal{S}_M$, $n = p, \dots, N$, by applying the time stepping scheme to equation (2.17), i.e., by

$$(2.25) \quad \sum_{i=0}^p \alpha_i \tilde{\mathbf{W}}^{n+i} + k\mathbf{A}\tilde{\mathbf{W}}^{n+p} = k \sum_{i=0}^{p-1} \gamma_i [\mathbf{B}_M(\tilde{\mathbf{W}}^{n+i}) + \mathbf{E}_M(t^{n+i})].$$

Then, according to Theorem 4.1 of Akrivis & Crouzeix (2004), see in particular relation (4.6) there, under the assumption

$$\max_{0 \leq t \leq T} \|\partial_t^j \mathbf{u}(\cdot, t)\| \leq C, \quad j = 1, \dots, p+1,$$

for a constant C , we have

$$(2.26) \quad \|\mathbf{W}(\cdot, t^n) - \tilde{\mathbf{W}}^n\|^2 + k \sum_{\ell=0}^n \|\mathbf{W}(\cdot, t^\ell) - \tilde{\mathbf{W}}^\ell\|^2 \leq Ck^{2p},$$

$n = p, \dots, N$. Therefore, in particular, we conclude that

$$(2.27) \quad \max_{0 \leq n \leq N} \|\mathbf{W}(\cdot, t^n) - \tilde{\mathbf{W}}^n\| \leq Ck^p$$

and, for k sufficiently small,

$$(2.28) \quad \max_{0 \leq n \leq N} \|\mathbf{W}_i(\cdot, t^n) - \tilde{\mathbf{W}}_i^n\| \leq \frac{1}{4}, \quad i = 1, 2.$$

In view of (2.23) and (2.27), it remains to estimate $\boldsymbol{\vartheta}^n := \tilde{\mathbf{W}}^n - \mathbf{U}^n$. Subtracting (2.16) from (2.25), we obtain

$$\sum_{i=0}^p \alpha_i \boldsymbol{\vartheta}^{n+i} + k\mathbf{A}\boldsymbol{\vartheta}^{n+p} = k \sum_{i=0}^{p-1} \gamma_i [\mathbf{B}_M(\tilde{\mathbf{W}}^{n+i}) - \mathbf{B}_M(\mathbf{U}^{n+i})] + k \sum_{i=0}^{p-1} \gamma_i \mathbf{E}_M(t^{n+i}).$$

Since on the right-hand side of (2.7) only the norm $\|\cdot\|$ appears, i.e., in the notation of Akrivis & Crouzeix (2004) we have $\lambda = 0$, and also $\beta(\zeta) = \zeta^p$, so that all coefficients of β but the one of ζ^p vanish, see Remark 7.2 in Akrivis & Crouzeix (2004), we may use the stability estimate (5.16') of Akrivis & Crouzeix (2004), to obtain

$$(2.29) \quad \|\boldsymbol{\vartheta}^n\|^2 + k \sum_{\ell=p}^n \|\boldsymbol{\vartheta}^\ell\|^2 \leq Ce^{c\mu^2 t^n} \left\{ \sum_{j=0}^{p-1} \|\boldsymbol{\vartheta}^j\|^2 + k \sum_{\ell=0}^{n-p} \|\mathbf{E}_M(t^\ell)\|_*^2 \right\},$$

provided that $\mathbf{U}^0, \dots, \mathbf{U}^{n-1} \in \mathbf{T}_u$. According to (2.20) and (2.18), there exists a constant C_* such that

$$(2.30) \quad Ce^{c\mu^2 T} \left\{ \sum_{j=0}^{p-1} \|\boldsymbol{\vartheta}^j\|^2 + k \sum_{\ell=0}^{N-p} \|\mathbf{E}_M(t^\ell)\|_*^2 \right\} \leq C_*^2 (k^p + M^{-m})^2.$$

The estimate (2.29) is obviously valid for $n = p$, since, according to (2.21), $\mathbf{U}^0, \dots, \mathbf{U}^{p-1} \in \mathbf{T}_u$. We next assume that it holds for $p, \dots, n-1$ with $p < n \leq N$. Then, according to (2.30) and the induction hypothesis, we have

$$\max_{p \leq j \leq n-1} \|\boldsymbol{\vartheta}_i^j\|_{L^\infty}^2 \leq c \max_{p \leq j \leq n-1} (\|\boldsymbol{\vartheta}_i^j\|^2 + \|\boldsymbol{\vartheta}_i^j\| \|(\boldsymbol{\vartheta}_i^j)_x\|) \leq C_*^2 (1 + k^{-1/2}) (k^p + M^{-m})^2;$$

thus, for k sufficiently small and $M^m k$ sufficiently large,

$$(2.31) \quad \max_{p \leq j \leq n-1} \|\boldsymbol{\vartheta}_i^j\|_{L^\infty} \leq \frac{1}{2}, \quad i = 1, 2.$$

From (2.24), (2.28) and (2.31) we obtain

$$(2.32) \quad \max_{p \leq j \leq n-1} \|\mathbf{u}_i(\cdot, t^j) - \mathbf{U}_i^j\|_{L^\infty}^2 \leq 1, \quad i = 1, 2,$$

and, thus, in view also of the assumption (2.21), that $\mathbf{U}^j \in \mathbf{T}_u$, $j = 0, \dots, n-1$. We conclude that (2.29) holds for n as well.

From (2.29) and (2.30), we easily conclude, for k sufficiently small and $M^m k$ sufficiently large,

$$(2.33) \quad \max_{0 \leq n \leq N} \|\tilde{\mathbf{W}}^n - \mathbf{U}^n\| \leq C(k^p + M^{-m}).$$

From (2.23), (2.27) and (2.33) the desired estimate (2.22) follows and the proof is complete. \square

REMARK 2.2 In our numerical experiments we also discretize the system

$$(2.34) \quad \begin{cases} H_t + \nu H_{xxx} + H_{xx} + HH_x + \Gamma_{xx} = f(x, t), \\ \Gamma_t - \eta \Gamma_{xx} + (H\Gamma)_x = g(x, t), \end{cases}$$

where $(x, t) \in \mathbb{R} \times [0, \infty)$. In this case the scheme (2.10) is modified by adding the terms $kf(t^{n+p})$ and $kg(t^{n+p})$ to their right-hand sides (p being the order of the scheme). Alternatively, f and g can be incorporated into the term \mathbf{B} .

REMARK 2.3 The results of this subsection can be easily extended to the general class of linearly implicit schemes considered in Akivis & Crouzeix (2004).

3. Numerical experiments

In this Section we implement the numerical schemes developed and analyzed above. The space discretization is performed using a spectral Fourier method and all six p -schemes are evaluated for accuracy by solving forced problems with known exact solutions. The numerical solutions are used to calculate the size of the strip of analyticity of the solutions of (1.6) and in addition, we carry out extensive numerical experiments as the parameter ν decreases and compute attractors with different characteristics including time- and quasi-periodic behavior as well as chaotic dynamics.

3.1 Discretization in space

The spatially 2π -periodic initial data assumption of the initial value problem enables us to represent the solution $\mathbf{u} = (H, \Gamma)$ of system (1.6) in the form

$$(3.1) \quad \begin{aligned} H(x, t) &= \sum_{j=1}^{\infty} (H_j^c(t) \cos jx + H_j^s(t) \sin jx) + \bar{H}(t), \\ \Gamma(x, t) &= \sum_{j=1}^{\infty} (\Gamma_j^c(t) \cos jx + \Gamma_j^s(t) \sin jx) + \bar{\Gamma}(t). \end{aligned}$$

The terms

$$\bar{H}(t) = \frac{1}{2\pi} \int_0^{2\pi} H(x, t) dx, \quad \bar{\Gamma}(t) = \frac{1}{2\pi} \int_0^{2\pi} \Gamma(x, t) dx$$

are independent of t due to the conservative nature of the system. Also, whenever $(H(x, t), \Gamma(x, t))$ is a solution, then so is $(H(x - ct, t) + c, \Gamma(x - ct, t))$, which allows us to remove $\bar{H}(t)$ from the problem. However, $\bar{\Gamma}$ cannot be removed from the problem and it is set by the initial conditions. In all the numerical experiments performed on (1.6) we take $\bar{\Gamma} = 2$, unless stated otherwise.

Substituting (3.1) in (1.6) we obtain

$$\begin{aligned} H_t + \nu H_{xxxx} + H_{xx} + HH_x + \Gamma_{xx} &= \sum_{j=1}^{\infty} \left(\frac{dH_j^c}{dt} + (\nu j^4 - j^2)H_j^c - j^2\Gamma_j^c - F_j^c \right) \cos jx \\ &+ \sum_{j=1}^{\infty} \left(\frac{dH_j^s}{dt} + (\nu j^4 - j^2)H_j^s - j^2\Gamma_j^s - F_j^s \right) \sin jx, \end{aligned}$$

and

$$\begin{aligned} \Gamma_t - \eta \Gamma_{xx} + (H\Gamma)_x &= \sum_{j=1}^{\infty} \left(\frac{d\Gamma_j^c}{dt} + \eta j^2\Gamma_j^c - G_j^c \right) \cos jx \\ &+ \sum_{j=1}^{\infty} \left(\frac{d\Gamma_j^s}{dt} + \eta j^2\Gamma_j^s - G_j^s \right) \sin jx, \end{aligned}$$

where

$$(3.2a) \quad F_j^c = -\frac{j}{2} \sum_{m+n=j} H_m^c H_n^s + \frac{j}{2} \sum_{m-n=j} (H_m^c H_n^s - H_n^c H_m^s),$$

$$(3.2b) \quad F_j^s = \frac{j}{4} \sum_{m+n=j} (H_m^c H_n^c - H_m^s H_n^s) + \frac{j}{2} \sum_{m-n=j} (H_m^c H_n^c + H_m^s H_n^s),$$

and

$$(3.2c) \quad G_j^c = j\bar{\Gamma}H_j^s + \frac{j}{2} \sum_{m+n=j} (\Gamma_m^c H_n^s + \Gamma_m^s H_n^c) - \frac{j}{2} \sum_{m-n=j} (\Gamma_m^c H_n^s - \Gamma_n^c H_m^s - \Gamma_m^s H_n^c + H_m^c \Gamma_n^s),$$

$$(3.2d) \quad G_j^s = -j\bar{\Gamma}H_j^c + \frac{j}{2} \sum_{m+n=j} (\Gamma_m^s H_n^c - \Gamma_m^c H_n^s) - \frac{j}{2} \sum_{m-n=j} (\Gamma_m^c H_n^c \Gamma_n^c H_m^c + \Gamma_m^s H_n^s + H_m^s \Gamma_n^s),$$

for $j \in \mathbb{N}$. System (2.1) is thus transformed into an infinite dimensional system of ordinary differential equations:

$$(3.3a) \quad \frac{dH_j^c}{dt} + \left(\lambda_j + \frac{1}{\nu}\right)H_j^c = \frac{1}{\nu}H_j^c + j^2\Gamma_j^c + F_j^c,$$

$$(3.3b) \quad \frac{dH_j^s}{dt} + \left(\lambda_j + \frac{1}{\nu}\right)H_j^s = \frac{1}{\nu}H_j^s + j^2\Gamma_j^s + F_j^s,$$

$$(3.3c) \quad \frac{d\Gamma_j^c}{dt} + \eta(j^2 + 1)\Gamma_j^c = \eta\Gamma_j^c + G_j^c,$$

$$(3.3d) \quad \frac{d\Gamma_j^s}{dt} + \eta(j^2 + 1)\Gamma_j^s = \eta\Gamma_j^s + G_j^s,$$

for $j \in \mathbb{N}$, where $\lambda_j = j^2 - \nu j^4$. The algebraic growth of the λ_j 's makes the system stiff.

Preliminary numerical experiments indicate that the solutions of (1.6) are analytic, and in fact, we obtained estimates for the strip of analyticity. (See Subsection 3.3.) In particular, the strip of analyticity (for any nonzero η) is proportional to $\nu^{1/2}$, and this provides a reasonable estimate for the truncation of the system, i.e., we can truncate the system at $C\nu^{-1/2}$, for a suitable constant C which depends on the desired accuracy. Notice that these estimates are consistent with those of the KS equation. (See Akrivis & Smyrlis 2004, Collet *et al* 1993a.) As a result, the nonlinear terms $(F_j^c, F_j^s, G_j^c, G_j^s)$ are truncated accordingly, i.e.,

$$F_j^{c,M} = -\frac{j}{2} \sum_{\substack{m+n=j \\ 1 \leq m, n \leq M}} H_m^c H_n^s + \frac{j}{2} \sum_{\substack{m-n=j \\ 1 \leq m, n \leq M}} (H_m^c H_n^s - H_n^c H_m^s),$$

with similar expressions for F_j^s, G_j^c and G_j^s .

In our numerical experiments we use the implicit–explicit BDF schemes (2.10) with

$$\mathbf{U} = (H_j^c, H_j^s, \Gamma_j^c, \Gamma_j^s)_{j=1}^M,$$

$$\mathbf{A}\mathbf{U} = \left(\left(\lambda_j + \frac{1}{\nu}\right)H_j^c, \left(\lambda_j + \frac{1}{\nu}\right)H_j^s, \eta(j^2 + 1)\Gamma_j^c, \eta(j^2 + 1)\Gamma_j^s \right)_{j=1}^M,$$

$$\mathbf{B}(\mathbf{U}) = \left(\frac{1}{\nu}H_j^c + j^2\Gamma_j^c + F_j^{c,M}, \frac{1}{\nu}H_j^s + j^2\Gamma_j^s + F_j^{s,M}, \eta\Gamma_j^c + G_j^{c,M}, \eta\Gamma_j^s + G_j^{s,M} \right)_{j=1}^M.$$

Order	$k = \frac{16}{10000}$	$k = \frac{8}{10000}$	$k = \frac{4}{10000}$	$k = \frac{2}{10000}$	$k = \frac{1}{10000}$
1	.1639e-00	.8261e-01	.4147e-01	.2077e-01	.1040e-01
2	.2488e-03	.6222e-04	.1556e-04	.3889e-05	.9723e-06
3	.3638e-06	.4548e-07	.5689e-08	.7153e-09	.1029e-09
Order	$k = \frac{400}{10000}$	$k = \frac{200}{10000}$	$k = \frac{100}{10000}$	$k = \frac{50}{10000}$	$k = \frac{25}{10000}$
4	.2014e-03	.1243e-04	.7723e-06	.4812e-07	.3007e-08
5	.7963e-05	.2345e-06	.7150e-08	.2218e-09	.7378e-11
6	–	–	.9685e-10	.4122e-11	.2370e-11

Table 1. Numerical implementation of all the schemes for a known solution: The maximum error in the L^2 -norm, i.e., $\max_{0 \leq n k \leq T} \|\mathbf{u}^n - \mathbf{U}^n\|$, where $T = 5$, of the approximate solution for various time steps is presented. The “–” corresponds to cases where the method did not yield satisfactory results.

In practice, the computations are based on the solution of a $4M$ by $4M$ stiff system of ODEs. Considering the truncated system of ODEs and in particular the evolution of the higher modes (large j), we see from the form of the nonlinear parts $\mathbf{B}(\mathbf{U})$ that nonlinear contributions are dominated by terms involving low frequency modes. This implies that higher frequencies are *slaved* to the low frequencies, which is one of the most typical characteristics of dissipative infinite dimensional dynamical systems. Nevertheless, we wish to allow as much freedom as possible to the high frequencies in order to develop individual behavior.

3.2 Accuracy tests for a known solution in a given time interval $[0, T]$

We have carried out tests to establish the p -th order accuracy, for $p \in \{1, 2, 3, 4, 5, 6\}$, of the corresponding p -step scheme for various time steps. These tests provide upper bounds for the time step which is required in order to achieve satisfactory accuracy; the numerical integration of each scheme was performed in the interval $[0, T]$. All these experiments approximate the solution of an *inhomogeneous* problem of the form

$$(3.4a) \quad \begin{cases} H_t + \nu H_{xxxx} + H_{xx} + HH_x + \Gamma_{xx} = f(x, t), \\ \Gamma_t - \eta \Gamma_{xx} + (H\Gamma)_x = g(x, t), \end{cases}$$

where $(x, t) \in \mathbb{R} \times [0, \infty)$, subject to suitable initial conditions

$$(3.4b) \quad \begin{cases} H(x, 0) = H_0(x), \\ \Gamma(x, 0) = \Gamma_0(x), \end{cases}$$

where $x \in \mathbb{R}$, with a known solution. All the functions f, g, H_0 and Γ_0 are 2π -periodic in space. The exact solution of (3.4) is taken to be

$$\begin{cases} H(x, t) = \sin(x+t), \\ \Gamma(x, t) = 2 - (1 - \nu) \cos(x+t), \end{cases}$$

which in turn provides $f(x,t)$, $g(x,t)$ through equation (3.4a). In all experiments T was chosen to be 5 whereas $\nu = 1/2$, $\eta = 1$ and the number of modes 24. This number was determined from preliminary experiments, see Subsection 3.3. Starting values for the different p -schemes are found using the exact solutions.

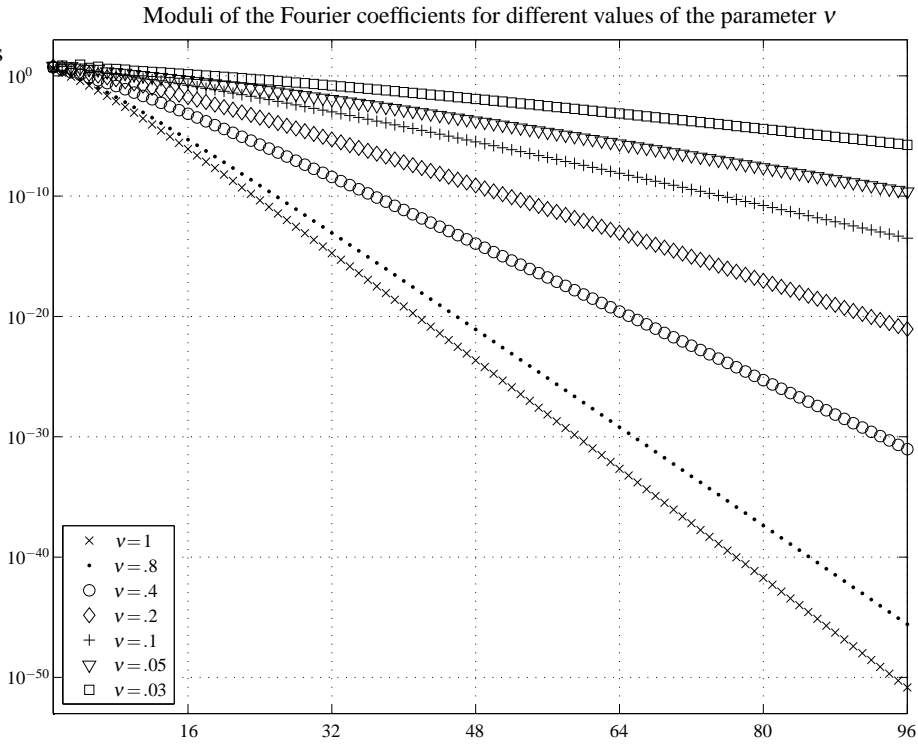


FIG. 1. The spectrum of the solution of system (1.6) as the parameter ν decreases. This $\log\log$ plot shows that the Fourier coefficients of the solution decay exponentially fast; slower decay rates are found as ν decreases.

In the case of the first, second and third order schemes, we used five different time steps, namely $k = \frac{16}{10000}, \frac{8}{10000}, \frac{4}{10000}, \frac{2}{10000}, \frac{1}{10000}$. In the case of the fourth, fifth and sixth order schemes we used the five time steps $k = \frac{400}{10000}, \frac{200}{10000}, \frac{100}{10000}, \frac{50}{10000}, \frac{25}{10000}$. We ran our experiments using a double precision FORTRAN code (without external subroutine calls) on an IBM-6000 workstation.

Table 1 contains all the maximum errors in the L^2 -norm, i.e.,

$$E = \max_{0 \leq nk \leq T} \|\mathbf{u}^n - \mathbf{U}^n\|,$$

over the interval $[0, T]$, for all six schemes and all six time steps. It can be observed from the results in Table 1 that each p -step method is of p -th order of accuracy, thus confirming numerically the theoretical predictions. In the case of the time steps $\frac{400}{10000}$ and $\frac{200}{10000}$ the 6-step method does not produce satisfactory results. When the 6-step method yields satisfactory results, the error is so small that it reaches machine precision (see Table 1).

ν	1.0	0.8	0.6	0.4	0.2	0.1	0.05
β	1.325	1.198	1.069	0.8435	0.5986	0.4143	0.4009
$\beta \nu^{-1/2}$	1.325	1.339	1.380	1.334	1.338	1.310	1.268

Table 2. Decay rate of the Fourier coefficients of the solutions.

k	Number of steps of the BDF-scheme					
	$p = 1$	$p = 2$	$p = 3$	$p = 4$	$p = 5$	$p = 6$
.0512	9.960416516	9.971680223	9.973643815	–	–	–
.0256	9.960616417	9.972883039	9.973288763	–	–	–
.0128	9.965503082	9.973154859	9.973244672	9.973238378	–	–
.0064	9.969026394	9.973218222	9.973239160	9.973238372	–	–
.0032	9.971047562	9.973233429	9.973238470	9.973238372	9.973238372	–
.0016	9.972121908	9.973237148	9.973238384	9.973238372	9.973238372	9.973238372
.0008	9.972674893	9.973238067	9.973238373	9.973238372	9.973238372	9.973238372
.0004	9.972955323	9.973238296	9.973238372	9.973238372	9.973238372	9.973238372
.0002	9.973096520	9.973238353	9.973238372	9.973238372	9.973238372	9.973238372
.0001	9.973167364	9.973238367	9.973238372	9.973238372	9.973238372	9.973238372
.00005	9.973202848	9.973238371	9.973238372	9.973238372	9.973238372	9.973238372

Table 3. The order of accuracy in the approximation of certain quantitative characteristics of the attractors: Calculations of the L^2 -norm of the solution in the case $\nu = .8$, $\eta = 1$ – a travelling wave – with different time steps k . The “–” corresponds to cases where the approximate solution did not converge to the attractor.

It is worth noting that the computational cost of BDF methods is independent of p , the number of steps in each method.

3.3 Decay of Fourier coefficients

We have carried out extensive numerical experiments in order to determine the number of modes that contribute numerically to the solution. In Figure 1 we depict the spectrum of the solutions of system (1.6) as ν decreases and for a fixed value of $\eta = 1$. The results clearly show that the values of

$$(3.5) \quad \mu_k = \limsup_{t \rightarrow \infty} |\hat{u}(k, t)|, \quad k \in \mathbb{Z},$$

decrease exponentially fast in $|k|$ and further analysis of the data suggests that a bound similar to (1.5) holds for (1.6). Using standard least-squares fitting of the μ_k 's in (3.5), we obtain that

$$\mu_k = \mathcal{O}(e^{-\beta|k|}), \quad k \in \mathbb{Z},$$

where β is a positive constant independent of k . However, β depends on ν and η , and in the case $\eta = 1$, our numerical experiments yield that $\beta \approx 1.3 \nu^{1/2}$. (See Table 2.) These experiments provide strong evidence that the solution of (1.6) is analytic and the band of analyticity is proportional to $\nu^{1/2}$, as is the case of the KS equation (Collet *et al* 1993a).

3.4 Travelling waves

Tests were carried out in order to demonstrate the p th order accuracy of the p -step method, for $p = 1, \dots, 6$, when evaluating certain quantitative characteristics of the attractors. For example we monitor the evolution of the L^2 -norm of the solution, defined by

$$(3.6) \quad E(t) = \left(|H(\cdot, t)|_{L^2(0, 2\pi)}^2 + |\Gamma(\cdot, t)|_{L^2(0, 2\pi)}^2 \right)^{1/2}.$$

For travelling wave states, the value of $E(t)$ is constant while in the case of a periodic attractor of period τ , the function E is τ -periodic. In particular, when $\nu = .8$, $\eta = 1$, there is a travelling wave global attractor, and in Table 3 we present values of the L^2 -norm of the solution as the time step is reduced for each of the p -step methods. It can be seen from the results that the p -step schemes, $p = 1, 2, 3$, provide corresponding orders of accuracy in the computed values of the L^2 -norms. On the other hand, analogous conclusion for the error of the p -step schemes, $p = 4, 5, 6$, cannot be drawn since they reach the 10-digit accuracy almost as soon as they provide convergent results.

3.5 Travelling-Periodic attractors

As the parameter ν decreases, the dimension of the global attractor increases. In the numerical experiments that follow we use the two-step method and set $\eta = 1$ while varying ν ; in addition $\bar{\Gamma} = 2$. For values of ν near 1, the attractor is a travelling wave, while near $\nu = .1$ it becomes a time-periodic attractor. We note that all computations presented here resulting in time-periodic behavior, produce solutions which are travelling-periodic, that is after each period of oscillation the solution returns to its original form but shifted horizontally by a constant amount, as shown in the results that follow. In Figure 3.5 we present results of the time periodic attractor when $\nu = .051$. The evolution of $H(x, t)$ and $\Gamma(x, t)$, in the (x, t) -plane, is depicted in Figures 2(a), 2(b), respectively. The results indicate that the solution is of a travelling time periodic type (the time periodicity is seen from the mild oscillations in the wave crests which would have been straight lines if the solutions were exactly travelling waves). Full evidence of the time periodicity of the solutions is provided in Figures 2(c)–2(d) which depict the evolution of the L^2 -norm of the solution along with the corresponding phase plane. The solution has period $\tau \approx 1.39199253021$ with $E(t)$ exhibiting six maxima and six minima over one period.

The period is calculated using a highly accurate technique which approximates $E(t)$ near values t^* where $E'(t^*) = 0$, by a suitable high order polynomial interpolation. The coefficients of the interpolant are determined through a weighted least squares method. The results of Figure 3.5, for example, were computed using an interpolating polynomial of degree six, the coefficients of which were determined from a least squares fit involving 17 suitably chosen consecutive pairs $(t_k, E(t_k))$. Newton's method is finally used to calculate an approximation to the root t^* of $E'(t)$. A desired number of consecutive local maxima and minima can therefore be calculated this way and the time-period of the solution follows from analyzing these data sets. Later in Section 3.6 we utilize the ordered sequence of minima to construct a return map that projects the infinite-dimensional dynamics to a map in \mathbb{R}^2 . In such constructions it is imperative to have an accurate calculation of the values of the minima if features such as folding and self-similarity or estimation of universal constants in period-doubling cascades are to be described (see Smyrlis & Papageorgiou (1991) for example).

Figures 2(c)–2(d) show the evolution and phase plane of the L^2 -norm after a long time so that the solution has been attracted to its time periodic orbit. We have also studied the effect of the different

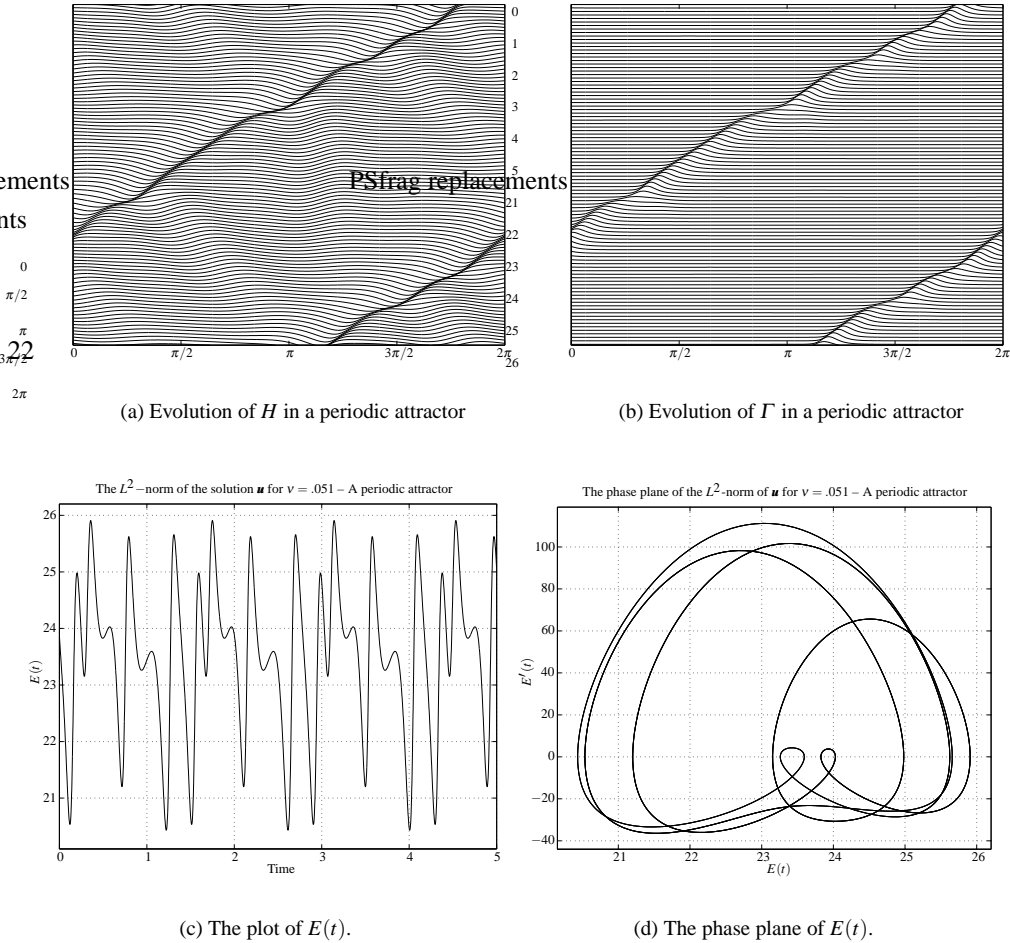


FIG. 2. Characteristics of the solution (H, Γ) in a periodic attractor – $\nu = .051, \eta = 1$.

p -step methods on the period τ of the solution and the results are completely in line with those of Table 3.

3.6 Transition to chaos

In this section we use the numerical schemes developed here for (1.6) to characterize attractors which are more complex dynamically than those computed earlier. All our computations fix $\eta = 1$ and vary ν . The dynamics become increasingly more complex as ν is decreased and our numerical work computes the most attracting solutions by solving initial value problems. Preliminary numerical experiments have identified some interesting transitions in the interval $\nu \in [.06700, .06950]$ as presented next.

Our numerical results imply that there is a quasi-periodic attractor at the largest value of $\nu = .06950$.

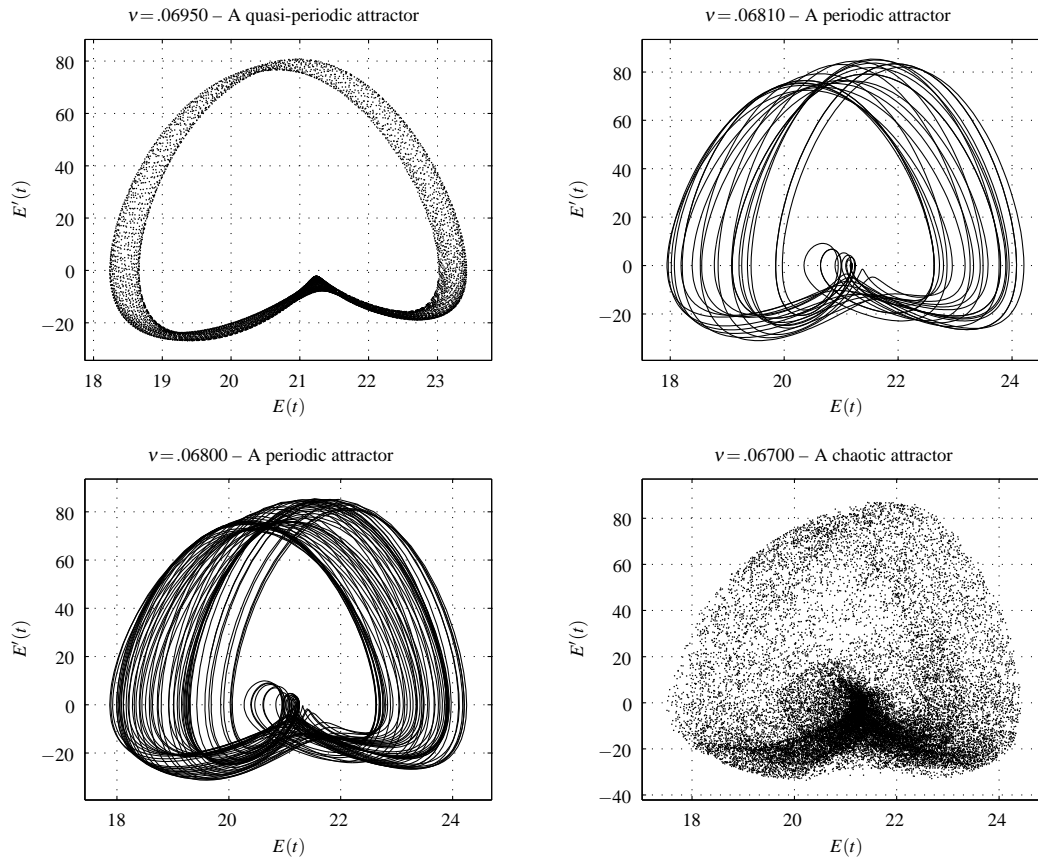


FIG. 3. Phase plane of the L^2 -norm: Transition from a quasi-periodic attractor to a periodic one to a period tripling to a chaotic attractor.

When ν is decreased to the values $.06810$ and $.06800$ the solution is attracted to a time-periodic attractor, and a further decrease to $\nu = .06700$ produces behavior which implies spatio-temporal chaos. The main tools we use here for the evaluation of these attractors are, (i) the construction of the phase plane of the L^2 -norm of the solution, i.e., the graph of $(E(t), E'(t))$ where t lies in a suitable interval and $E(t)$ is given by (3.6), and, (ii) the construction of the *Return Map* of the minima of $E(t)$, i.e., the set of points $(m_\ell, m_{\ell+1})$, for sufficiently large ℓ , with $m_\ell, m_{\ell+1}$ consecutive minima of $E(t)$. In the cases where the phase plane curves are not closed (e.g., for the quasi-periodic and chaotic examples) we depict the phase-plane trajectories with discrete points rather than joining them, in order to avoid the significant amount of overlapping curves that would emerge otherwise and which would dominate the figure without providing a sense for the geometry of the attractor.

In Figure 3 we present the phase planes of the L^2 -norm of the solution for the four parameters $\nu = .06950, .06810, .06800, .06700$ as indicated on the figures. When $\nu = .06950$ (upper left panel) the system (1.6) possesses a quasi-periodic attractor. The phase plane is not a closed curve and strong evidence of the quasi-periodicity of the dynamics is furnished by the return map of the minima of $E(t)$. This map is given in Figure 4(a) and it is clearly seen that these Poincaré sections produce a closed

curve which is typical of quasi-periodic dynamics on a torus. We note that the ability of our numerical methods to produce such sharp objects in \mathbb{R}^2 is due to the accuracy of both the p -schemes and the method of calculation of the minima $\{m_\ell\}$ that are used to construct the return maps.

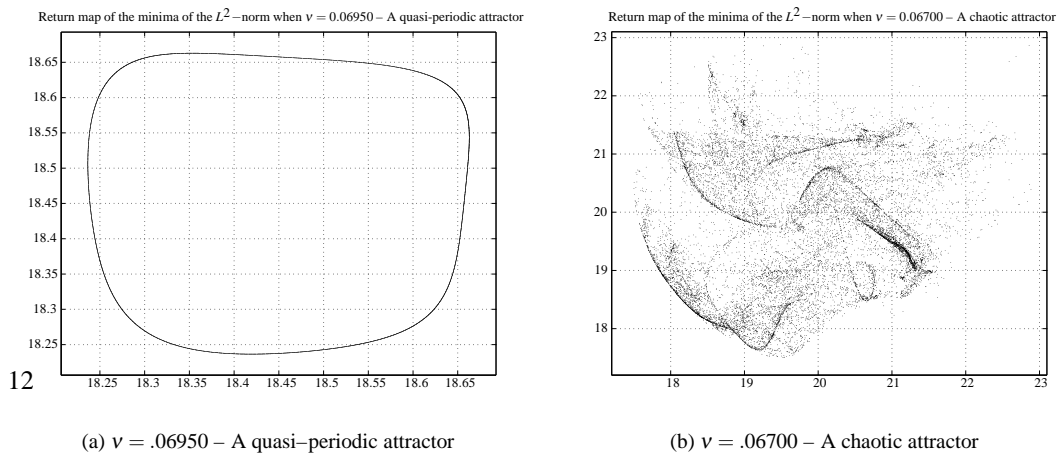


FIG. 4. When $\nu = .06950$, the return map of the minima lives in a closed curve while when $\nu = .06700$, the return map of the minima creates a cloud in the plane.

When ν is decreased a bit the most strongly attracting manifold is a time-periodic attractor. Evidence for this is given in the top right and bottom left panels of Figure 3 that correspond to $\nu = .06810$ and $.06800$, respectively. Both phase planes are closed curves that consist of 26 and 72 turns, respectively (the results shown in Figure 3 represent a large time of integration which is a large multiple of the basic period of oscillation, so that each phase plane contains many turns which lie on top of each other – once more the comments given earlier with regard to the need for a high level of accuracy are relevant here also). In fact, for $\nu = .06810$ the period is $\tau = 8.7717201126$ and in one period $E(t)$ possesses 26 minima, while for $\nu = .06800$ the period is $\tau = 24.431110924$ and in one period $E(t)$ possesses 72 minima. There is strong evidence that the dynamics has undergone a period tripling.

Finally, we reduce ν further to the value $.06700$ where our numerical experiments suggest that the system (1.6) possesses a chaotic attractor. The phase plane is given in the bottom right panel of Figure 3 and the corresponding return map of the minima in Figure 4(b). Clearly, the phase plane is not a closed curve indicating aperiodic behavior and the geometry of the return map leads us to surmise that the dynamics are chaotic. The return map of the minima of $E(t)$ creates a *cloud* in a bounded region of the plane, which contains certain sharp features including folding (note that the solution is sampled after a sufficiently large time has passed so that transients are expected to have died out). We classify such dynamics as chaos with no recognizable patterns as opposed to, for example, chaos that emerges from a period-doubling cascade following the Feigenbaum scenario. Such “unrecognizable” dynamics have been found in related computations by the authors, see for example Coward, Papageorgiou & Smyrlis (1995), Papageorgiou & Smyrlis (1991), Smyrlis & Papageorgiou (1996).

An example of the foliations in the return map of the minima of $E(t)$, which are typical in chaotic dynamics of KS type equations, is included in Figures 5(a) and 5(b). We take $\nu = .06799$ and $\eta = 1$,

where chaotic dynamics are found. The return map is given in Figure 5(a) and an enlargement of the boxed region in the vicinity of the point (20, 10) is depicted in the right panel, Figure 5(b). Foliations and self-similarity of the attractor is strongly evident in these results and such qualitative behavior has been established by the authors in computations of the KS equation also - see references above. We have not attempted a numerical estimate of the fractal dimension of the return map but expect this to be a number between 1 and 2.

4. Conclusions

We have analyzed, implemented and carried out extensive numerical experiments for a system of semi-linear parabolic equations that arise in core-annular two-fluid flows in the presence of surfactants. The coupled system reduces to the Kuramoto–Sivashinsky equation in a special limit and our work is concerned with the analysis and computation of such evolution equations. We apply a class of implicit–explicit BDF schemes and assuming the existence of solutions we prove convergence of the numerical approximations. The class of p -schemes for $p = 1, \dots, 6$ has been successfully implemented and the order of accuracy of the schemes has been fully confirmed numerically by computing characteristics of the solutions in different attractors. Following a referee’s suggestion we make some comments regarding variable time stepping for multistep schemes. The stability of such schemes is quite delicate and results are mostly known for the zero stability of the implicit two-step BDF scheme (see Crouzeix & Lisbona (1984), Calvo *et al* (1990)), along with some preliminary results for the absolute stability of the same scheme (Thomé (2006)), and preliminary results concerning the zero stability of higher order schemes (Calvo *et al* 1990).

The schemes are applicable to a wider class of parabolic systems and in future work we will extend our work to consider dispersive effects (the system (1.6) can be extended to include a term H_{xxx} on the left hand side of the first equation to yield a dispersion–modified parabolic system – see Kas–Danouche *et al* 2009).

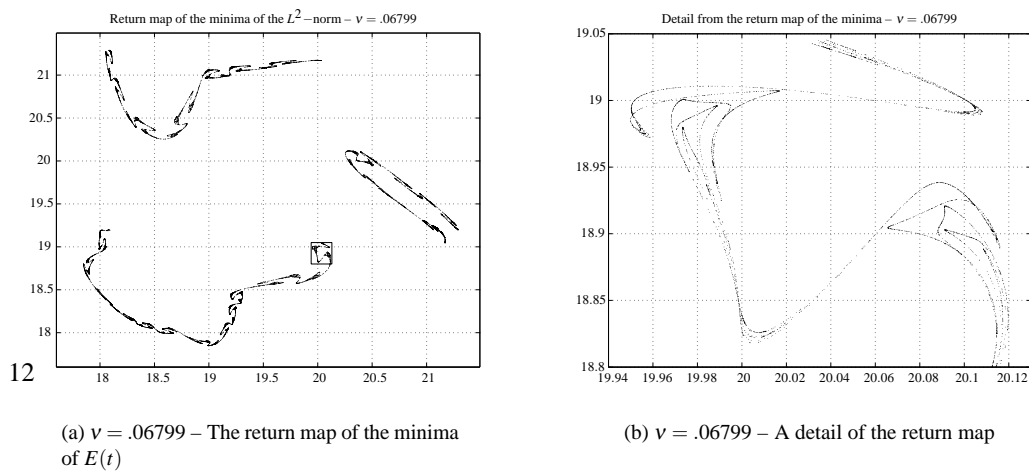


FIG. 5. Foliations in the return map of the minima, when $v = .06799$.

Acknowledgements

Parts of this work were undertaken while GA and DTP were Visiting Professors in the Department of Mathematics and Statistics, University of Cyprus.

Funding

This work of DTP was partly supported by grant number DMS–0707339 from the National Science Foundation. The work of YSS was supported by a grant from the University of Cyprus.

Appendix

For $p = 1, \dots, 6$, the schemes (2.10) for the system

$$\mathbf{u}_t + \mathbf{A}\mathbf{u} = \mathbf{B}(\mathbf{u}),$$

subject to the initial condition

$$\mathbf{u}(x, 0) = \mathbf{u}_0(x),$$

take the following form

$$(A.1) \quad \mathbf{U}^{n+1} + k\mathbf{A}\mathbf{U}^{n+1} = \mathbf{U}^n + k\mathbf{B}(\mathbf{U}^n),$$

$$(A.2) \quad \frac{3}{2}\mathbf{U}^{n+2} + k\mathbf{A}\mathbf{U}^{n+2} = 2\mathbf{U}^{n+1} - \frac{1}{2}\mathbf{U}^n + 2k\mathbf{B}(\mathbf{U}^{n+1}) - k\mathbf{B}(\mathbf{U}^n),$$

$$(A.3) \quad \begin{aligned} \frac{11}{6}\mathbf{U}^{n+3} + k\mathbf{A}\mathbf{U}^{n+3} &= 3\mathbf{U}^{n+2} - \frac{3}{2}\mathbf{U}^{n+1} + \frac{1}{3}\mathbf{U}^n \\ &+ 3k\mathbf{B}(\mathbf{U}^{n+2}) - 3k\mathbf{B}(\mathbf{U}^{n+1}) + k\mathbf{B}(\mathbf{U}^n), \end{aligned}$$

$$(A.4) \quad \begin{aligned} \frac{25}{12}\mathbf{U}^{n+4} + k\mathbf{A}\mathbf{U}^{n+4} &= 4\mathbf{U}^{n+3} - 3\mathbf{U}^{n+2} + \frac{4}{3}\mathbf{U}^{n+1} - \frac{1}{4}\mathbf{U}^n \\ &+ 4k\mathbf{B}(\mathbf{U}^{n+3}) - 6k\mathbf{B}(\mathbf{U}^{n+2}) + 4k\mathbf{B}(\mathbf{U}^{n+1}) - k\mathbf{B}(\mathbf{U}^n), \end{aligned}$$

$$(A.5) \quad \begin{aligned} \frac{137}{60}\mathbf{U}^{n+5} + k\mathbf{A}\mathbf{U}^{n+5} &= 5\mathbf{U}^{n+4} - 5\mathbf{U}^{n+3} + \frac{10}{3}\mathbf{U}^{n+2} - \frac{5}{4}\mathbf{U}^{n+1} + \frac{1}{5}\mathbf{U}^n \\ &+ 5k\mathbf{B}(\mathbf{U}^{n+4}) - 10k\mathbf{B}(\mathbf{U}^{n+3}) + 10k\mathbf{B}(\mathbf{U}^{n+2}) - 5k\mathbf{B}(\mathbf{U}^{n+1}) + k\mathbf{B}(\mathbf{U}^n), \end{aligned}$$

$$(A.6) \quad \begin{aligned} \frac{147}{60}\mathbf{U}^{n+6} + k\mathbf{A}\mathbf{U}^{n+6} &= 6\mathbf{U}^{n+5} - \frac{15}{2}\mathbf{U}^{n+4} + \frac{20}{3}\mathbf{U}^{n+3} - \frac{15}{4}\mathbf{U}^{n+2} \\ &+ \frac{6}{5}\mathbf{U}^{n+1} - \frac{1}{6}\mathbf{U}^n + 6k\mathbf{B}(\mathbf{U}^{n+5}) - 15k\mathbf{B}(\mathbf{U}^{n+4}) \\ &+ 20k\mathbf{B}(\mathbf{U}^{n+3}) - 15k\mathbf{B}(\mathbf{U}^{n+2}) + 6k\mathbf{B}(\mathbf{U}^{n+1}) - k\mathbf{B}(\mathbf{U}^n). \end{aligned}$$

Scheme (A.1) is obviously a combination of the implicit and forward Euler methods. Starting values for each p -scheme are produced by other p -accurate schemes, for example Runge–Kutta methods.

REFERENCES

- AKRIVIS, G. & CROUZEIX, M. (2004) Linearly implicit methods for nonlinear parabolic equations, *Math. Comp.*, **73**, 613–635.
- AKRIVIS, G., CROUZEIX, M. & MAKRIDAKIS, C. (1998) Implicit–explicit multistep finite element methods for nonlinear parabolic problems, *Math. Comp.*, **67**, 457–477.
- AKRIVIS, G., CROUZEIX, M. & MAKRIDAKIS, C. (1999) Implicit–explicit multistep methods for quasilinear parabolic equations, *Numer. Math.*, **82**, 521–541.
- AKRIVIS, G. & SMYRLIS, Y.–S. (2004) Implicit–explicit BDF methods for the Kuramoto–Sivashinsky equation, *Appl. Numer. Math.*, **51**, 151–169.
- CALVO, M., GRANDE, T. & GRIGORIEFF, R.D. (1990) On the zero stability of the variable order variable stepsize BDF-formulas, *Numer. Math.*, **57**, 39–50.
- COLLET, P., ECKMANN, J.–P., EPSTEIN, H. & STUBBE, J. (1993a) Analyticity for the Kuramoto–Sivashinsky equation, *Phys. D*, **67**, 321–326.
- COLLET, P., ECKMANN, J.–P., EPSTEIN, H. & STUBBE, J. (1993b) A global attracting set for the Kuramoto–Sivashinsky equation, *Comm. Math. Phys.*, **152**, 203–214.
- CONSTANTIN, P., FOIAS, C., NICOLAENKO, B. & TEMAM, R. (1989) *Integral manifolds and inertial manifolds for dissipative partial differential equations*, New York: Springer–Verlag.
- COWARD, A. V., PAPAGEORGIOU, D. T. & SMYRLIS, Y.–S. (1995) Nonlinear stability of oscillatory core–annular flow: a generalized Kuramoto–Sivashinsky equation with time periodic coefficients, *Z. Angew. Math. Phys.*, **46**, 1–39.
- CROUZEIX, M. & LISBONA, F.J. (1984) The convergence of variable-stepsize, variable-formula, multistep methods, *SIAM J. Numer. Anal.*, **21**, 512–534.
- DIECI, L., JOLLY, M. S., ROSA, R. & VAN VLECK, E. S. (2008) Error in approximation of Lyapunov exponents on inertial manifolds: the Kuramoto–Sivashinsky equation, *Discrete Contin. Dyn. Syst. Ser. B*, **9**, 555–580.
- GOODMAN, J. (1994) Stability of the Kuramoto–Sivashinsky and related systems, *Comm. Pure Appl. Math.*, **47**, 293–306.
- HYMAN, J. M. & NICOLAENKO, B. (1986) The Kuramoto–Sivashinsky equation: a bridge between PDEs and dynamical systems, *Phys. D*, **18**, 113–126.
- HYMAN, J. M., NICOLAENKO, B. & ZALESKI, S. (1986) Order and complexity in the Kuramoto–Sivashinsky model of weakly turbulent interfaces, *Phys. D*, **23**, 265–292.
- IL’YASHENKO, JU. S. (1992) Global analysis of the phase portrait for the Kuramoto–Sivashinsky equation, *J. Dynam. Differential Equations*, **4**, 585–615.
- JOLLY, M. S., KEVREKIDIS, I. G., & TITI, E. S. (1990) Approximate inertial manifolds for the Kuramoto–Sivashinsky equation: analysis and computations, *Phys. D*, **44**, 38–60.
- JOSEPH, D. D. & RENARDY, Y. Y. (1993) *Fundamentals of two–fluid dynamics. Part II*, New York: Springer–Verlag.
- KAS–DANOUCHE, S., PAPAGEORGIOU, D. T. & SIEGEL, M. (2009) Nonlinear dynamics of core–annular film flows in the presence of surfactants, *J. Fluid Mechanics*, **626**, 415–448.
- KEVREKIDIS, I. G., NICOLAENKO, B. & SCOVEL, J. C. (1990) Back in the saddle again: a computer assisted study of the Kuramoto–Sivashinsky equation, *SIAM J. Appl. Math.*, **50**, 760–790.
- PAPAGEORGIOU, D. T. & SMYRLIS, Y.–S. (1991) The route to chaos for the Kuramoto–Sivashinsky equation, *Theoret. Comput. Fluid Dynamics*, **3**, 15–42.
- SMYRLIS, Y.–S. & PAPAGEORGIOU, D. T. (1991) Predicting chaos for infinite–dimensional dynamical systems: the Kuramoto–Sivashinsky equation, a case study, *Proc. Nat. Acad. Sci. U.S.A.*, **88**, 11129–11132.
- SMYRLIS, Y.–S. & PAPAGEORGIOU, D. T. (1996) Computer assisted study of strange attractors of the Kuramoto–Sivashinsky equation, *Z. Angew. Math. Mech.*, **76**, 57–60.

- THOMÉE, V. (2006) *Galerkin finite element methods for parabolic problems*, second ed., Springer Series in Computational Mathematics, v. 25, Berlin.
- ZGLICZYŃSKI, P. (2004) Rigorous numerics for dissipative partial differential equations. II. Periodic orbit for the Kuramoto-Sivashinsky PDE—a computer-assisted proof, *Found. Comput. Math.*, **4**, 157–185.
- P. ZGLICZYŃSKI & MISCHAIKOW, K. (2001) Rigorous numerics for partial differential equations: the Kuramoto-Sivashinsky equation, *Found. Comput. Math.*, **1**, 255–288.